

## Introducing a Sub-cell Tensor Technique into a (2, 4) FDTD Method

R.S. Schechter, S.T. Chun, M.S. Kluskens, M. Kragalott, and D. A. Zolnick

Authors are in Code 5310 of the Radar Division of the Naval Research Laboratory, Washington DC 20375  
richard.schechter@nrl.navy.mil

**Abstract:** A sub-cell tensor based technique for modeling dielectric interfaces is introduced into a (2,4) FDTD method. For each cell containing an interface, a tensor based method that enforces continuity conditions is used to determine the fields on both sides the sloped interface. These fields are then volumetrically averaged. The approach is used to calculate a corrected field value at each grid point of the large fourth-order stencil. The combined algorithm is computationally homogeneous, unlike most previous algorithms of this type, and thus lends itself to parallel processing. Additionally, the method may be used with other higher-order stencils. The accuracy is tested using the exact Mie series solution for scattering from a dielectric sphere. It is shown that using the (2,4) tensor method results in ~50-70% less error than the (2,4) standard Yee method in the vicinity of a dielectric sphere.

**Introduction:** The finite-difference time domain (FDTD) method is one of the most widely employed methods in computational electromagnetics. As it has been pointed out in many articles, the method has problems when there are curved boundaries, which are represented by staircases on a Cartesian grid. If continuity conditions are not properly maintained across these curved interfaces, inaccuracies in the field components can occur. Nadobny et. al. [1] developed a 3D tensor method for the treatment of dielectric interfaces to enforce continuity of the appropriate field components. Their paper was a major extension of the work of Lee and Myung [2] and demonstrated much improved accuracy for the standard (2,2) algorithm.

In this paper we adapt the tensor method for use with fourth-order methods. Fourth and other higher order methods permit modeling on coarser grids. This is important because fourth-order methods, although very accurate in homogeneous regions, generally present accuracy problems at material boundaries. One remedy for this problem

is to employ a hybrid formulation of (2,4) FDTD and sub-grid (2,2) FDTD methods [3], where (2,4) stands for second-order accurate in time and fourth-order accurate in space. In [3] a coarse (2,4) grid is used in the homogeneous regions and a finer (2,2) sub-grid near conducting walls and other structures. Another method [4] uses a large (2,4) region and a buffer layer of (2,2) cells between the (2,4) region and the interfaces.

In [5] an efficient higher-order alternating-direction implicit (ADI) finite-difference time-domain method for unconditionally stable analysis of curvilinear electromagnetic compatibility (EMC) problems is presented. The method is practically dispersionless and offers improved accuracy for curved boundaries. Another paper [6] also discusses the reduction of numerical dispersion of the finite-difference time-domain method based on a (2,4) computational stencil. Rather than implementing the conventional approach, based on Taylor analysis for the determination of the finite-difference operators, two alternative procedures that result in numerical schemes with diverse wide-band behavior are proposed. The method is shown to outperform the standard (2,4) method.

The method proposed here uses the same (2,4) algorithm and grid spacing for the homogenous regions and across boundaries as opposed to mixing different accuracy (second and fourth-order) algorithms. This is important for parallel processing, i.e. using the Message Passing Interface (MPI), where having a homogeneous algorithm is a great advantage so that each processor executes the same instructions. It also is an advantage computationally if a fourth-order accurate method can be used to model an electrically large structure on a smaller coarser grid, without any special sub-gridding. We gauge the relative accuracy of the standard Yee fourth-order and combined sub-cell tensor fourth-order methods by comparing computed results with the exact Mie series solution for plane waves scattering from a dielectric sphere.

**Sub-cell Tensor Method:** The differential form of Maxwell's equations is given by:

$$\nabla \times \mathbf{E} = -\mu \frac{\partial \mathbf{H}}{\partial t}, \quad (1)$$

$$\nabla \times \mathbf{H} = \frac{\partial \mathbf{D}}{\partial t} + \mathbf{J}, \quad (2)$$

where

$$\mathbf{D} = \varepsilon \mathbf{E}. \quad (3)$$

In the homogeneous cells, where there are no interfaces, Eq. (3) can be used to obtain  $\mathbf{E}$ . However, in those cells with interfaces, boundary conditions must be explicitly satisfied.

At a dielectric interface these continuity conditions must be maintained at the interface between media 1 and 2:

$$(\varepsilon_1 \mathbf{E}_1 - \varepsilon_2 \mathbf{E}_2) \cdot \mathbf{n} = 0, \quad (4)$$

(Continuity of the normal components of  $\mathbf{D}$ ),

$$(\mathbf{E}_1 - \mathbf{E}_2) \times \mathbf{n} = 0, \quad (5)$$

(Continuity of the tangential components of  $\mathbf{E}$ ),

where  $\mathbf{n}$  is the unit normal vector to the interface.

Eqs. (4) and (5) can be solved for  $\mathbf{E}_2$  in terms of  $\mathbf{E}_1$ :

$$\mathbf{E}_2 = \tilde{\mathbf{A}} \mathbf{E}_1 \quad (6)$$

where the elements of the transformation matrix  $\tilde{\mathbf{A}}$  are:

$$a_{11} = n_x^2 \left( \frac{\varepsilon_1}{\varepsilon_2} \right) + n_y^2 + n_z^2,$$

$$a_{12} = n_x n_y \left( \frac{\varepsilon_1}{\varepsilon_2} - 1 \right),$$

$$a_{13} = n_x n_z \left( \frac{\varepsilon_1}{\varepsilon_2} - 1 \right),$$

$$a_{21} = a_{12},$$

$$a_{22} = n_x^2 + n_y^2 \left( \frac{\varepsilon_1}{\varepsilon_2} \right) + n_z^2,$$

$$a_{23} = n_y n_z \left( \frac{\varepsilon_1}{\varepsilon_2} - 1 \right),$$

$$a_{31} = a_{13},$$

$$a_{32} = a_{23},$$

$$a_{33} = n_x^2 + n_y^2 + n_z^2 \left( \frac{\varepsilon_1}{\varepsilon_2} \right).$$

For Yee cell faces cut by an interface the electric fluxes through the faces are broken into two parts:

$$\begin{aligned} \iint D_x dS &= \varepsilon_1 E_x^1 S_x^1 + \varepsilon_2 E_x^2 S_x^2, \\ \iint D_y dS &= \varepsilon_1 E_y^1 S_y^1 + \varepsilon_2 E_y^2 S_y^2, \\ \iint D_z dS &= \varepsilon_1 E_z^1 S_z^1 + \varepsilon_2 E_z^2 S_z^2, \end{aligned} \quad (7)$$

where the  $S$ 's are areas and the superscripts stand for side 1 or 2. This is illustrated in Fig. 1.

Combining Eqs. (6) with (7), the following tensor relationship is obtained between the average electric flux density and electric field in medium 1,

$$\tilde{\mathbf{D}} = \tilde{\boldsymbol{\varepsilon}} \cdot \mathbf{E}_1 \quad (8)$$

where  $\tilde{\boldsymbol{\varepsilon}}$  is a 3 by 3 permittivity tensor with components:

$$\varepsilon_{11} = \varepsilon_1 \left( \frac{S_x^1}{S} \right) + \varepsilon_2 \left( \frac{S_x^2}{S} \right) a_{11},$$

$$\varepsilon_{12} = \varepsilon_2 \left( \frac{S_x^2}{S} \right) a_{12},$$

$$\varepsilon_{13} = \varepsilon_2 \left( \frac{S_x^2}{S} \right) a_{13},$$

$$\varepsilon_{21} = \varepsilon_2 \left( \frac{S_y^2}{S} \right) a_{21},$$

$$\varepsilon_{22} = \varepsilon_1 \left( \frac{S_y^1}{S} \right) + \varepsilon_2 \left( \frac{S_y^2}{S} \right) a_{22},$$

$$\varepsilon_{23} = \varepsilon_2 \left( \frac{S_y^2}{S} \right) a_{23},$$

$$\varepsilon_{31} = \varepsilon_2 \left( \frac{S_z^2}{S} \right) a_{31},$$

$$\varepsilon_{32} = \varepsilon_2 \left( \frac{S_z^2}{S} \right) a_{32},$$

$$\varepsilon_{33} = \varepsilon_1 \left( \frac{S_z^1}{S} \right) + \varepsilon_2 \left( \frac{S_z^2}{S} \right) a_{33},$$

and where  $S = S^1 + S^2$ .

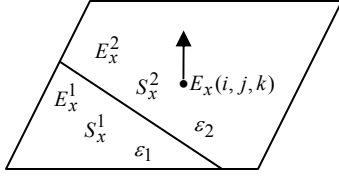


Fig. 1. Center slice (face) of Yee cell centered around  $E_x(i, j, k)$ . There are two flux areas separated by the dielectric interface.

At each point in the stencil for updating the  $H$  field components the volume average of the  $E$  fields is used. The fourth-order update equation for  $H_z$  obtained by discretizing Eq. 1 is:

$$H_z^{n+1/2}(i, j, k) = H_z^{n-1/2}(i, j, k) + \frac{r}{24} \times$$

$$[(-\bar{E}_x^n(i, j+2, k) + 27\bar{E}_x^n(i, j+1, k) - 27\bar{E}_x^n(i, j, k) + \bar{E}_x^n(i, j-1, k)) -$$

$$(-\bar{E}_y^n(i+2, j, k) + 27\bar{E}_y^n(i+1, j, k) - 27\bar{E}_y^n(i, j, k) + \bar{E}_y^n(i-1, j, k))]$$
(9)

where  $r = \frac{\Delta t}{\Delta x \mu_0}$  and for example,

$$\bar{E}_x = \frac{(V_1 E_x^1 + V_2 E_x^2)}{V}, \quad V = V_1 + V_2, \quad (10)$$

where  $V_1$  and  $V_2$  are the volumes on sides one and two of the interface. It should be noted that Eq. (9) is identical in form to the standard (2,4) update equation, the only difference being that each term is replaced by the volume averaged field. There are analogous update equations for  $H_x$  and  $H_y$ .

Standard fourth-order update equations for  $D_x$ ,  $D_y$  and  $D_z$  may be obtained by discretizing Eq. 2. For example:

$$\bar{D}_y^{n+1}(i, j, k) = \bar{D}_y^n(i, j, k) + \frac{s}{24} \times$$

$$[(-H_x^{n+1/2}(i, j, k+1) + 27H_x^{n+1/2}(i, j, k) - 27H_x^{n+1/2}(i, j, k-1) + H_x^{n+1/2}(i, j, k-2)) -$$

$$(-H_z^{n+1/2}(i+1, j, k) + 27H_z^{n+1/2}(i+1, j, k) - 27H_z^{n+1/2}(i-1, j, k) + H_z^{n+1/2}(i-2, j, k))]$$
(11)

where  $s = \frac{\Delta t}{\Delta x \epsilon_0}$ .

The term  $\bar{E}_x(i, j, k)$  in Eq. (9) represents the volume averaged field in the Yee cell centered on  $E_x(i, j, k)$ . For any point in the stencil with an interface in that cell, Eq. (10) is used to correct for

the interface. This concept is illustrated in Fig. 2. If there is no interface, then

$$\bar{E}_x = \frac{\bar{D}_x}{\epsilon}. \quad (12)$$

This algorithm amounts to using a corrected field value at each point in the stencil to account for any interfaces cutting through the stencil volume in an arbitrary way. If the stencil volume has no interfaces the algorithm reduces to the standard (2,4). The entire algorithm may be briefly summarized as follows for one update:

[1] Perform standard (2,4) update of  $\bar{\mathbf{D}}$  using  $H_x$ ,  $H_y$  and  $H_z$ .

[2] Test all 8  $E$  cells for interfaces within the fourth-order stencil for updating  $H$ .

If  $E$  cell has an interface then use the sub-cell tensor method:

(a) Compute electric field from average electric flux density,  $\mathbf{E}_1 = \tilde{\boldsymbol{\epsilon}}^{-1} \cdot \bar{\mathbf{D}}$ .

(b) Obtain electric field on other side of interface,  $\mathbf{E}_2 = \tilde{\mathbf{A}} \mathbf{E}_1$ .

(c) Volume average electric field,

$$\bar{E}_x = \frac{(V_1 E_x^1 + V_2 E_x^2)}{V}$$

else if the  $E$  cell has no interface then,

(a) Compute electric field from  $\bar{E}_x = \frac{\bar{D}_x}{\epsilon}$

[3] Perform standard (2,4) update for  $\mathbf{H}$  using  $\bar{E}_x$ ,  $\bar{E}_y$ , and  $\bar{E}_z$ .

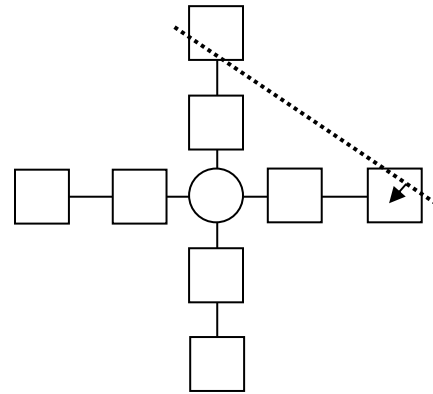


Fig. 2. The stencil for the (2,4) FDTD method showing the 8  $E$  field cells (squares) and  $H$  field cell (circle). Two of the  $E$  field cells are cut by an interface (dotted line) at an angle and require the sub-cell corrections.

**Computational Cases:** Six computational cases are performed to test the accuracy of the standard (2,4) and tensor (2,4) algorithms. Scattering problems are done with a plane wave scattering from a dielectric sphere with a large dielectric change to emphasize errors near the interface. The incident plane wave is polarized in the z direction and travels in the +y direction, as illustrated in Fig. 3. The total-field/scattered-field (TF/SF) formulation is used to introduce a plane wave into the volume. Uniaxial perfectly matched layers (UPML), 10 cells wide, are used for the absorbing boundaries. Case I uses a sphere with a relative dielectric constant of 4 and a uniform grid spacing of 10 points per wavelength (ppw) in the sphere. The parameters for various cases are summarized in Table I.

**Table I. Parameters for Cases.**

	Freq. (GHz)	Dielectric Constant	ppw	Sphere Radius
Case I	5.0	4	10	7.5
Case II	5.0	4	20	15.0
Case III	5.0	8	10	7.5
Case IV	5.0	8	20	15.0
Case V	5.0	12	10	7.5
Case VI	5.0	12	20	15.0

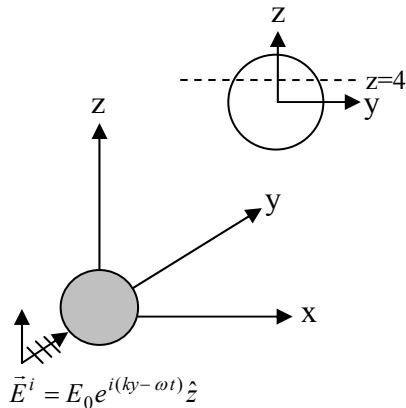


Fig. 3. Diagram of incident wave, dielectric sphere, coordinate system and y-cut at z value.

Fig. 4 shows a typical computed cut for Case III, parallel to the y-axis and through grid point ( $x=0, z=1$ ), near the sphere center. Shown is  $E_y(0, y, 1)$  computed using the (2,4) tensor method and the (2,4) standard Yee method against the exact Mie series solution. Fig. 4 shows that the (2,4) tensor method agrees much better with the exact solution than the (2,4) standard method, along the entire cut.

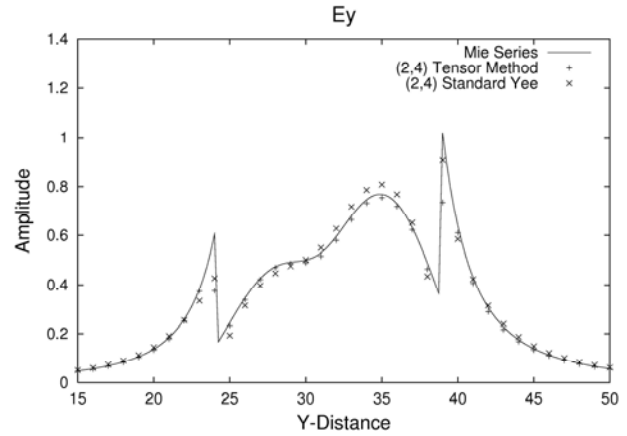


Fig. 4. Case III. Comparison of (2,4) tensor and (2,4) standard methods with exact Mie series. The sphere lies between grid points 24 and 40.

Fig. 5 shows a comparable cut for  $E_y(0, y, 5)$  for Case V. The (2,4) tensor method is closer to the exact solution inside the sphere, at the sphere boundaries, and outside the sphere. The standard Yee method also exhibits pronounced overshoots at the interfaces.

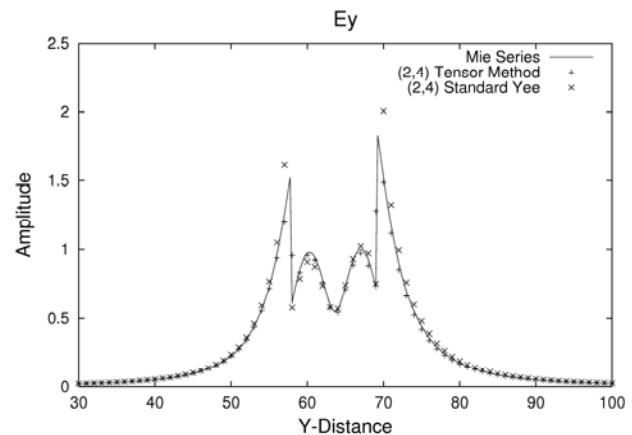


Fig. 5. Case V. Comparison of (2,4) tensor and (2,4) standard methods with exact Mie series. The sphere lies between grid points 56 and 72.

**Error Evaluation:** In order to assess the relative errors of the tensor and standard methods a numerical comparison is made between the computed values and the exact Mie series solution. The solution is computed in spherical coordinates and transformed into Cartesian coordinates along cuts through the sphere (shown in Fig. 3), to correspond in space to the FDTD spatial cuts.

The following error measure function is used:

$$error = \frac{\sum |E_{exact} - E_{computed}|}{\sum |E_{exact}|} \quad (13)$$

This error function is computed along a cut through the sphere and extending 1 radius beyond the sphere boundary on both sides so that the cuts are 4 radii in length. The exact value is taken to be the average of the analytical value at center of the Yee cell, obtained from the Mie series solution. Using the spatial average of the exact solution is necessary near the jump discontinuities to properly compare to the computed values which are really the average values at the center of the Yee cells. Table II shows the errors computed for the six cases along y-cuts at 4 different z values for increasing dielectric constants. The ratio r shown is the tensor average error divided by the standard average. Table II shows that r is about 0.3 at 20 ppw and .6 at 10 ppw for the six cases. Cases II and IV both show a decrease of about 50% in the average error by going from 10 ppw to 20 ppw for the tensor method. The standard method shows worse convergence. Case VI shows only about a 20% decrease in the average error by going to 20 ppw.

**Table II. Errors for Cases I – VI.**

Case I	ez(1)	ez(4.5)	ey(1)	ey(4)	av.
ten(2,4)	1.79	2.30	2.31	2.11	2.13
sta(2,4)	1.94	3.53	4.85	4.06	3.60
					r=.59
Case II	ez(1)	ez(8.5)	ey(1)	ey(8)	av.
ten(2,4)	0.61	0.88	1.46	0.98	0.98
sta(2,4)	1.80	1.78	4.83	4.41	3.21
					r=.31
Case III	ez(1)	ez(4.5)	ey(1)	ey(4)	av.
ten(2,4)	3.98	5.62	2.54	3.13	3.82
sta(2,4)	6.67	11.30	6.99	5.68	7.66
					r=.50
Case IV	ez(1)	ez(8.5)	ey(1)	ey(8)	av.
ten(2,4)	2.15	2.16	1.94	1.48	1.93
sta(2,4)	4.64	4.95	6.26	7.00	5.71
					r=.34
Case V	ez(1)	ez(4.5)	ey(1)	ey(4)	av.
ten(2,4)	3.45	3.25	2.77	3.26	3.18
sta(2,4)	3.86	5.33	8.31	5.32	5.71
					r=.56
Case VI	ez(1)	ez(8.5)	ey(1)	ey(8)	av.
ten(2,4)	2.66	2.90	2.67	1.67	2.48
sta(2,4)	5.87	3.55	8.48	8.88	6.70
					r=.37

**Efficiency:** The (2,4) tensor is compared with the (2,4) standard Yee for total CPU time and additional memory requirements. The computations were all performed on an IBM p690 parallel computer using 16 processors. This case uses a grid size of 168×168×168 and 2000 time steps. The (2,4) tensor method uses 373 s of CPU time compared to 251s for the (2,4) standard Yee, or a ratio of 1.49. The tensor method also requires some additional memory primarily to store the  $9 \tilde{\epsilon}^{-1}$  tensor components and the 9 transformation matrix components of the  $\tilde{A}$  matrix for each interface cell. For this case there are 786 interface cells for each of the staggered field positions  $E_x$ ,  $E_y$  and  $E_z$ . Also the volume fractions must be stored for each interface cell. The total additional memory overhead compared with the standard (2,4) method amounts to only about 0.2 Mbytes for this case.

**Conclusions:** A tensor method to handle dielectric interfaces has been combined in a straightforward way with a standard (2,4) FDTD algorithm and results in a computationally homogeneous algorithm suitable for parallel computing. The numerical cases, using scattering from a dielectric sphere, demonstrate that the combined (2,4) tensor method significantly improves the accuracy of the (2,4) standard Yee method near interfaces. The tensor method may be combined with any higher-order FDTD algorithm, involving a large stencil.

## References

- [1] J. Nadobny, D. Sullivan, W. Wlodarczyk, P. Deuflhard, and P. Wust, "A 3-D Tensor FDTD-Formulation for Treatment of Sloped Interfaces in Electrically Inhomogeneous Media," *IEEE Trans. Antenn. Prop.*, Vol 51, No.8, pp. 1760-1770, Aug. 2003.
- [2] J. Lee and N. Myung, "Locally Tensor Conformal FDTD Method for Modeling Arbitrary Dielectric Surfaces," *Microwave and Optical Technology Letters*, Vol. 23, No. 4, pp. 245-249, Nov. 1999.
- [3] S. V. Georgakopoulos, C. R. Birtcher, C. A. Balanis, and R. A. Renaut, "Higher-Order Finite-Difference Schemes for Electromagnetic Radiation, Scattering, and Penetration, Part 2: Applications," *IEEE Antenna's and Propagation Magazine*, Vol. 44, No. 2. pp. 92-101, April 2002.
- [4] M. F. Hadi and M. Piket-May, "A Modified FDTD (2,4) Scheme for Modeling Electrically Large Structure with High-Phase Accuracy," *IEEE Trans. Antenna. Prop.*, Vol. 45, No. 2, pp. 254-264, Feb. 1997.

- [5] N. V. Kantartzis, T.T. Zygiridis, T. D. Tsiboukis, "An Unconditionally Stable Higher Order ADI-FDTD Technique for the Dispersionless Analysis of Generalized 3-D EMC Structures," *IEEE Trans. Magn.*, Vol. 40, No. 2, pp. 1436-1439, March 2004.
- [6] T. T. Zygiridis and T.D. Tsiboukis, "Low-Dispersion Algorithms Based on the Higher Order (2,4) FDTD Method," *IEEE Trans. MTT*, Vol. 52, No. 4, pp. 1321-1327, April 2004.



Richard Schechter is a physicist in the Radar Division at Naval Research Laboratory in Washington DC. His current interests are the finite-difference time domain method, parallel computing, and modeling electromagnetic bandgap structures and left-handed materials. He also has conducted research and published articles on simulating ultrasonic wave propagation on parallel computers. He obtained his B.S. in Physics from the University of Maryland in 1974 and took further graduate studies in physics and applied mathematics 1974-1980 at American University and Catholic University, both in Washington DC.



Michael S. Kluskens received B.S. and M.S. degrees in electrical engineering from Michigan Technological University, Houghton, MI, in 1984 and 1985, respectively, and the Ph.D degree from The Ohio State University, Columbus, OH, in 1991. From 1986 to 1991, he was a Graduate Research Associate at the ElectroScience Laboratory, Department of Electrical Engineering, the Ohio State University, where he conducted research on the method of moments and chiral media. He has been with the Radar Division of the Naval Research Laboratory, Washington D.C. since 1991 and is currently with the Electromagnetics Section of the Analysis Branch of the Radar Division. His primary research is in computational electromagnetics with emphasis on the method of moments, finite-difference time domain, and scattering from large complex structures.



Mark Kragalott received the B.A. degree in physics and economics at Kenyon College in 1983, and M.S. and Ph.D. degrees in electrical engineering from The Ohio State University, in 1988 and 1993, respectively. As a Graduate Research Associate at the ElectroScience Laboratory at The Ohio State University, he conducted research on method of moments and extremely low frequency shielding. Since 1994 he has been with the Electromagnetics Section in the Analysis Branch of the Radar Division at the Naval Research Laboratory, Washington, D.C, where he has conducted research in topics ranging from computational electromagnetics to ultrawideband radiation and scattering.



Sung-Taek Chun received the B.A.N.E degree from Han-Yang University, Seoul, Korea, in 1980, and studied theoretical plasma physics at the Seoul National University in 1981. He received the M.S and Ph.D. degrees in Nuclear Engineering and Engineering Physics from University of Wisconsin-Madison in 1984 and 1986, respectively. From 1987 to 1989, he was a Research Associate in the Courant Institute of Mathematical Sciences, New York University, N.Y. During 1997 and 1999, he was an Associate Professor in Physics in Taejon, Korea, and since 2001, he has been a Research Physicist at the Naval Research Laboratory, Washington, DC. His research interests include theoretical and computational electromagnetics and plasma physics, photonic bandgap materials, RF and pulse discharge plasma, and electromagnetic wave interaction with charged particles and complex media.